ELSEVIER

The impact of hydrochemical boundary conditions on the evolution of limestone karst aquifers

Douchko Romanov[a], Franci Gabrovsek[b], Wolfgang Dreybrodt[a],*

[a]*Karst Processes Research Group, Institute of Experimental Physics, University of Bremen, Postfach 330410 (NW1 Kufsteiner Str), D-28334 Bremen, Germany*
[b]*Karst Research Institute, ZRC SAZU, Postojna, Slovenia*

Abstract

The early evolution of karst aquifers depends on a manifold of initial and boundary conditions such as geological setting, hydrologic properties of the initial aquifer, and petrologic properties of the rock. When all water entering at various inputs into the aquifer has equal chemical composition with respect to the system $H_2O-CO_2-CaCO_3$ early evolution under conditions of constant head exhibits breakthrough (BT) behaviour. If the chemical compositions of the input waters are different, deep in the aquifer where the saturated solutions mix renewed aggressiveness occurs, and additional dissolutional widening of fractures by mixing corrosion (MC) changes the hydrologic properties of the aquifer. To study the impact of MC on the evolution of karst we have modelled a simple karst aquifer consisting of a confined limestone bed, with two symmetrically located inputs at constant head and open flow conditions along the entire width at base level. To calculate dissolutional widening of the fractures the well-known dissolution kinetics of limestone was used, which is linear up to 90% of saturation with respect to calcite and then switches to a nonlinear fourth order rate law. First, two extremes are modelled: (a) Both inputs receive aggressive water of equal chemical composition with $[Ca^{2+}] = 0.75[Ca^{2+}]_{eq}$. In this case two channels migrate downstream with that from one input more competitive and reaching base level first, causing BT. (b) Water at both inputs is saturated with respect to calcite, but in equilibrium with different partial pressures of CO_2. Therefore, dissolution widening can occur only where these waters mix. A central channel starts to grow extending down-head until base level is reached. Flow rates through the aquifer first rise and become constant after the channel has reached base level. In the following runs these two extreme modes of karstification are combined. The waters entering have different chemical compositions and therefore different equilibrium concentrations $[Ca^{2+}]_{eq}$. This allows MC to be active. They are also undersaturated with the inflowing solutions at concentration $[Ca^{2+}]_{in} = f[Ca^{2+}]_{eq}$ where f is the ratio of saturation. In comparison to the extreme limit (a) the action of MC now creates permeability where the solutions mix and diverts the evolution of conduits into this region. Finally one conduit reaches base level and causes BT. This behaviour is found for $f = 0.7$, 0.9, and 0.96.

For solutions more close to equilibrium with respect to calcite ($f = 0.99$, 0.9925, and 0.995) BT behaviour is replaced by a steady increase in flow rates. In the early state as in the case of MC controlled evolution (case b) a central channel not connected to the input is created by MC and reaches base level. After this event, further increase in flow rates is caused by slow dissolutional widening by the slightly undersaturated input solutions flowing towards the central channel.

---

* Corresponding author. Tel.: +49-421-218-3556; fax: +49-421-218-7318.

 E-mail addresses: dreybrod@physik.uni-bremen.de (W. Dreybrodt), dromanov@physik.uni-bremen.de (D. Romanov), gabrovsek@zrc-sazu.si (F. Gabrovsek).

Comparison of the various model aquifers at termination of the computer runs reveals significant differences in their properties caused solely by changes of the hydrochemical boundary conditions.

1. Introduction

Karst is a characteristic geological feature of areas comprised of limestone. Due to the solubility of these rocks in water, containing carbon dioxide karst aquifers which exhibit an extreme heterogeneity of hydraulic conductivities have developed from initial narrow joints, fissures, and partings. Karst conduits with diameters from about 1 cm up to the order of 10 m drain water from the aquifer, the storage of which is effected mainly in narrow fissures with aperture widths below 1 mm down to several tens of micrometers (Worthington et al., 2000). These fissures constitute most of the porosity of the aquifer, which in classical karst areas amounts to a few percent of the total rock volume. Hydraulic conductivities in such aquifers range between 10^{-8} and 10^{-5} m s^{-1} in the fracture systems, and up to 1 m s^{-1} in the conduits. Much of the present knowledge on karst aquifers in fissured rocks is summarized in textbooks by Ford and Williams (1989) and White (1988).

Karst aquifers due to their complex structure respond in an unexpected way to drawdown of groundwater, rain storms, or input of contaminant material. Therefore detailed information on their hydrogeological properties is of utmost importance in facilitating risk assessment. One way to understand the evolution of karst aquifers is by computer modelling approaches which have been put forward during the last two decades (Palmer, 1984, 1991, 1999, 2000; Dreybrodt, 1988, 1990, 1996; Siemers and Dreybrodt, 1998; Dreybrodt and Siemers, 2000; Dreybrodt and Gabrovsek, 2000; Gabrovsek and Dreybrodt, 2001; Groves and Howard, 1994; Howard and Groves, 1995; Clemens et al., 1997, 1999; Kaufmann and Braun, 1999, 2000).

All these computer models have in common one most important ingredient. This basic element is the dissolution kinetics of limestone by CO_2 containing water flowing in initially narrow fractures with aperture widths on the order of 0.01 cm. The dissolution rates have been obtained experimentally and follow a linear rate law far away from equilibrium, but then switch to a higher order kinetics above a switch concentration c_s at about 80–90% of saturation with respect to calcite (Svensson and Dreybrodt, 1992; Eisenlohr et al., 1999; Dreybrodt and Eisenlohr, 2000). These rates can be formulated by

$$F = k_1(1 - c/c_{\text{eq}}) \text{ for } c < c_s = 0.9c_{\text{eq}}$$

$$F = k_n(1 - c/c_{\text{eq}})^n \text{ for } c \geq c_s = 0.9c_{\text{eq}} \tag{1}$$

where c is the concentration of calcium in the solution and c_{eq} is its equilibrium value with respect to calcite. k_1 and k_n are rate constants in mol cm^{-2} s^{-1} with typical values of 4×10^{-11} and 4×10^{-8}, respectively, n takes values of about 4.

In its earliest stage karstification proceeds under constant head conditions, where the calcite aggressive solution is driven by a constant hydraulic head difference h through initially narrow fractures with aperture width a_0 and length ℓ. Due to dissolutional widening the average aperture width $a(t)$ of the fracture increases with time t. The dissolution rate at the output of such a fracture is given (Dreybrodt and Gabrovsek, 2000) by

$$F(\ell, t) = k_n \left(1 - \frac{c_{\text{in}}}{c_{\text{eq}}}\right)^n \left\{ \frac{\ell a_0^3}{L_n a^3(t)} + 1 \right\}^{-n/(n-1)} \tag{2}$$

$$L_n = \frac{\rho g a_0^3 b_0 h c_{\text{eq}} M_0}{24 \eta (n-1) \ell k_n (1 - c_{\text{in}}/c_{\text{eq}})^{n-1}(a_0 + b_0)} \tag{3}$$

where ρ is the density of water and η its dynamic viscosity, c_{in} is the concentration of the inflowing solution, b_0 is the width of the fracture, M_0 is a geometric constant in the order of one, g is gravitational acceleration.

As long as the ratio $\ell a_0^3 / L_n a^3(t) \gg 1$ in Eq. (2), a positive feedback mechanism determines the evolution of the aperture width, because increasing aperture width $a(t)$ enhances the dissolution rate and vice versa. As a consequence initial widening and

corresponding flow rates through the fracture are low but increase steadily until a dramatic and sudden rise occurs at breakthrough (BT) time T, which is given by

$$T[\text{years}] = \frac{1}{2\gamma} \frac{n-1}{2n+1} \frac{a_0}{F(\ell, 0)} \tag{4}$$

where $\gamma = 1.17 \times 10^9$ converts the dissolution rates to wall retreat in cm/year. This BT occurs when the exit of the fracture has been widened to about twice its initial value. All models of karst aquifers incorporate this basic process and by this way are successful to explain karstification under various conditions in its scale on space and time.

In most modelling efforts the input concentration c_{in} was either zero or well below c_s. If, however, for some reason water entering into a rock massif is close to saturation, well above c_s the feed back mechanism is switched off and dissolutional widening becomes even and extremely slow everywhere in the initial aquifer (Dreybrodt and Gabrovsek, 2000). This can be seen from Eqs. (3) and (2). If c_{in} approaches c_{eq}, L_n approaches infinity. Therefore $(\ell a_0^3/L_n a^3(t)) \ll 1$ in Eq. (2) and the rates are given by $F(\ell, t) = k_n(1 - c_{\text{in}}/c_{\text{eq}})^n$. In such a case the permeability of the aquifer increases slowly in time. For $c_{\text{in}} = 0.99$ the rate of wall retreat is 4×10^{-7} cm/year, and for $c_{\text{in}} = 0.995 c_{\text{eq}}$, 2.5×10^{-8} cm/year, respectively. Even a moderate increase of hydraulic conductivity would need several hundred thousand to millions of years in such cases, to double the fracture aperture width.

A second conduit forming mechanism then becomes relevant. This is the well-known concept of mixing corrosion, referred as MC further on in this paper. If two saturated (or almost saturated) $H_2O-CO_2-CaCO_3$ solutions with different equilibrium concentrations with respect to calcite are mixed, the solution becomes undersaturated (Laptev, 1939; Bögli, 1980) and renewed dissolution becomes active. Gabrovsek and Dreybrodt (2000) in a first modelling attempt have shown for a confluence of two fractures injecting water of differing equilibrium concentrations into a third outflow fracture, that the combination of MC and nonlinear kinetics considerably enhances karstification, compared to that of nonlinear kinetics solely. They have applied these results to a two-dimensional network with two input points, with solutions entering with zero calcium concentration but differing p_{CO_2}. Deep in the aquifer

these solutions are almost saturated. In the region where they mix, MC becomes active creating increased permeability. This redirects conduits already growing from the inputs, creating different BT patters compared to those which would originate if both inputs have equal p_{CO_2}, i.e. MC were absent.

In this paper we investigate the action of MC more systematically on a refined modelling technique allowing better spatial resolution and taking into account the statistical distribution of fracture aperture widths. Furthermore, we systematically investigate the influence of the calcium concentration at the inputs. (a) Two extremes are possible. The input solutions are chemically equal and only BT behaviour results. (b) The inflowing solutions are at equilibrium with respect to calcite, but differ in c_{eq}. In this case only MC becomes active inside the aquifer, where a conduit grows on a much longer time scale downhead without exhibiting BT of flow rates.

If the input concentrations are varied for both inputs to $c_{\text{in}} = fc_{\text{eq}}$ where $0.75 < f < 1$, denotes the degree of saturation, both mechanisms, BT and MC are active. For $f < 0.96$ BT behaviour dominates. For $f > 0.96$ MC gains influence and the BT behaviour is suppressed. In all these cases a channel develops inside the aquifers without connection to the inputs.

By this way, with respect to our earlier work which represents only one specific case where BT behaviour proved to be dominant, we now cover the full region of interaction of BT behaviour and MC.

2. Model structure

The idealized model domain, depicted in Fig. 1 consists of a limestone bed 1 m in depth, 500 m long, and 255 m wide. It is dissected by fractures into blocks of $5 \times 5 \times 1$ m^3. The aperture widths of the narrow fractures separating these blocks are statistically distributed by a lognormal relation with average aperture width $a_0 = 0.015$ cm, and $\sigma = 0.01$. There are two inputs A and B with a hydraulic head, $h = 25$ m, at the left hand side, which otherwise is impermeable, as indicated by the black rim. The lower and upper boundaries are also impervious. The right hand side is open to flow at a head of $h = 0$ m. The aperture widths of the lognormal realisation are given
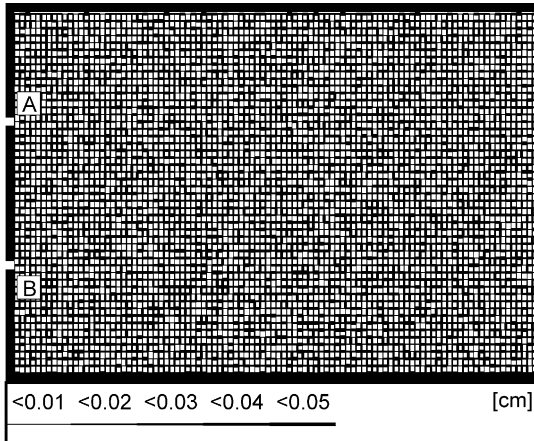
Fig. 1. Model domain with realization of the log-normally distributed aperture widths of fractures as given by the bar code below. The length is 500 m, the width is 255 m. The two input points A and B are at a head of 25 m, the right hand side boundary is open to flow at head zero. All other boundaries are impervious as indicated by the black rim.

by the thicknesses of the lines as depicted by the bar code below.

Water entering into the inputs is allowed for different chemical composition of the solution. The chemical composition of these solutions is characterized in the following way: We assume a calcium-free initial solution in equilibrium with an initial $p^i_{CO_2}$. When this solution dissolves limestone it consumes one molecule CO_2 for each $CaCO_3$ dissolved, and attains equilibrium at some c_{eq}. The actual concentration of CO_2 in a solution with Ca-concentration c is therefore given by

$$[CO_2] = [CO_2]_i - c \tag{5}$$

We now characterize the solution, entering into the inputs at the left hand side by $[CO_2]_i = K_H p^i_{CO_2}$ and $c = f c_{eq}$. K_H is Henry's constant, $f < 1$ gives the percentage of saturation at the corresponding $p^i_{CO_2}$. As long as the $p^i_{CO_2}$ at the two inputs are different MC is active. If $p^i_{CO_2}$ is equal at both inputs MC is switched off (Gabrovsek and Dreybrodt, 2000). Comparison between these two cases allows judgement of the effect of MC on the evolution of the aquifer. We assume dissolution kinetics with $c_s = 0.9c_{eq}$, $k_1 = 4 \times 10^{-11}$ mol cm^{-2} s^{-1}, $n = 4$, $k_4 = 4 \times 10^{-8}$ mol cm^{-2} s^{-1} (cf. Eq. (1)). These

values are typical for limestone (Dreybrodt and Eisenlohr, 2000). The temperature of the solutions has been fixed at 10 °C.

3. Calculation of the network evolution

To obtain widening of each fracture element connecting two nearest nodes i and j the heads h_i and h_j must be known, and furthermore the chemical composition of the inflowing solution with respect to Ca and CO_2. Flow through the fractures is obtained by use of the Hagen–Poiseuille equation which connects the head difference $h_i - h_j$ to the flowrate Q_{ij} through the fracture (i, j). By this way one finds a set of linear equations from which all the heads are calculated. Once the flow rates are known dissolutional widening is calculated by applying the dissolution-transport-equation (Dreybrodt, 1996; Gabrovsek, 2000) first to all fractures connected to input points. Then the concentrations of Ca and CO_2 and along this fractures are calculated. Furthermore the new widths profile after timestep Δt is obtained. In the next step we select all nodes, where the concentrations of the input solutions are known. We assume complete mixing of these solutions. Then, as described above the concentration profiles and new widths profiles are found. This procedure is repeated downhead for all remaining fractures. For the new network after time Δt the new flow rates are calculated and the procedure is repeated. In all calculations presented in the following sections flow remained laminar as confirmed by a Reynold number below 2000. For details of the procedure see Dreybrodt (1996), Siemers and Dreybrodt (1998), and Gabrovsek (2000).

4. Results

We first discuss the two extreme limits.

(a) No MC is active and only BT behaviour results.
(b) The inflowing solutions are at equilibrium with respect to calcite and to $p^i_{CO_2}$ which are different at inputs A and B. Only where they mix can MC become active and thus can permeability be increased.
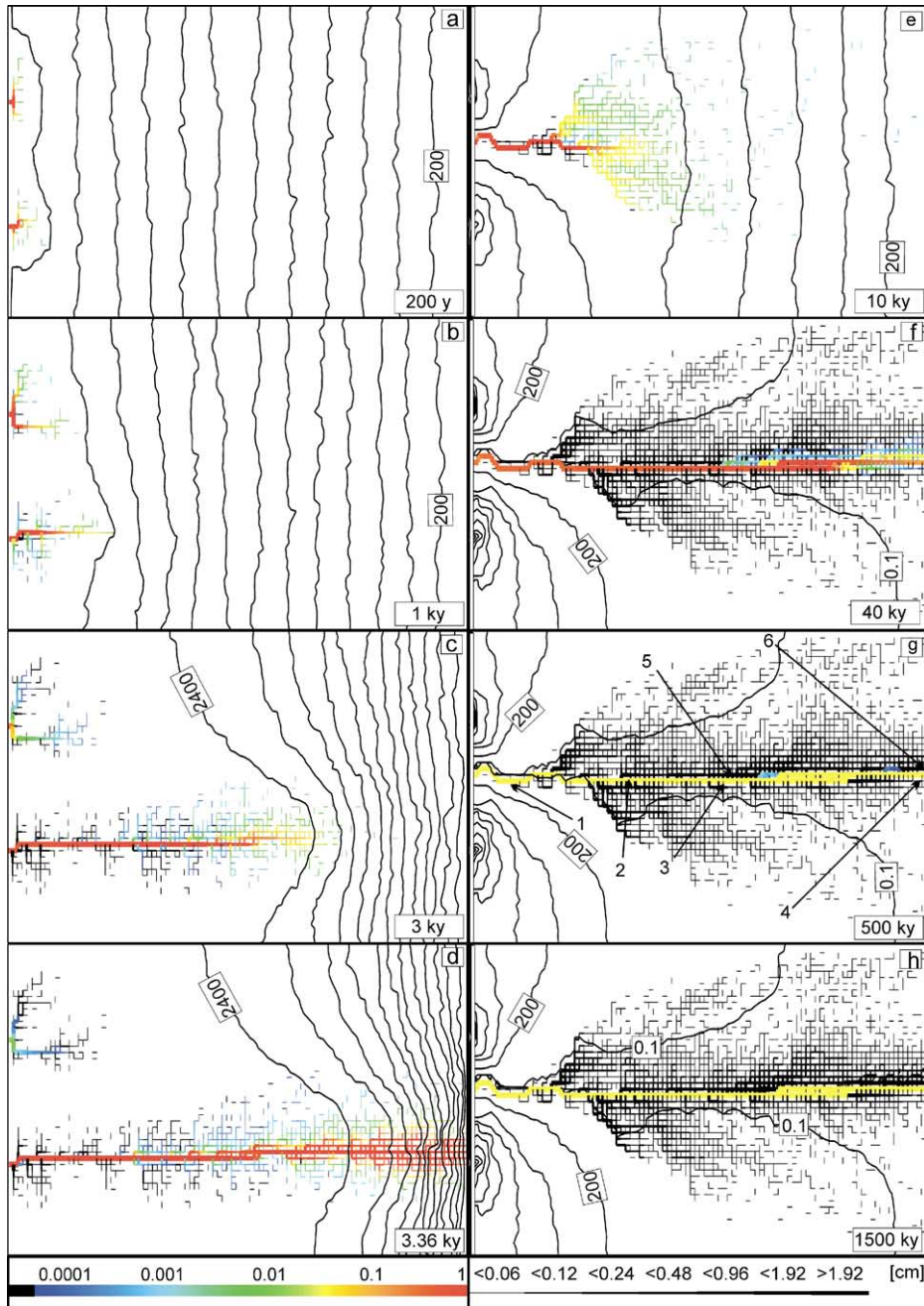
Fig. 2. Evolution of dissolution rates and fracture widths for the two extreme limits of BT (a–d) and pure MC (e–h). The isolines of head are given in distances of 200 cm. The times of evolution are given at the lower corner of the right hand sides. The dissolution rates are depicted in colours as in the colour code in units of maximal dissolution rates during the evolution. Black denotes rates smaller than $10^{-5}\,F_{max}$. $F_{max} = 0.0034$ cm/year for a–d, and $F_{max} = 1.6 \times 10^{-4}$ cm/year for e–f (MC). The fracture widths are given in cm by the bar code below. No fractures with aperture widths below 0.06 cm are shown. Note that the bar code is not linear, but in geometrical progression. The fattest bars show fractures with aperture widths larger than 1.92 cm. The other numbers show the range of aperture widths represented by the corresponding bar.

Fig. 2 depicts the results for comparison. Fig. 2a–d shows the evolution of the aquifer, when both solutions entering at the input have equal chemical compositions ($p_{CO_2}^i = 5 \times 10^{-2}$ atm, $c_{in} = 0.75c_{eq}$, $c_{eq} = 2.14 \times 10^{-6}$ mol cm^{-3}). Therefore MC is not active. The figures show all fractures with aperture widths larger than 0.06 cm, thus presenting only regions where dissolutional widening exerts strong effects (note that the bar code is different from that of Fig. 1). We also show the distribution of the hydraulic heads as isolines, to visualize flow in the net. The colours designate the dissolution rates in a logarithmic scale, where red is the maximal rate F_{max}, dark blue stands for 0.0001 F_{max}. Black stands for dissolution rates $< 10^{-5}F_{max}$. Fig. 2a shows the initial situation 200 years after onset of karstification. As one can see from the isolines of the hydraulic heads flow radiates out from the input points and after some 10 m is distributed evenly downstream towards the output. Conduits start to grow from the inputs. After 1000 years (Fig. 2b) these conduits have progressed further downstream. After 3000 years, the lower channel has deeply penetrated into the aquifer, whereas the upper one has not changed significantly (Fig. 2c). Due to the deep penetration of the lower channel the heads are redistributed to attract more flow into this channel. After only further 360 years (Fig. 2d) the conduit has reached the output and BT occurs. During the entire evolution of the aquifer the dissolution rates drop along the flow-path from the entrance to the exit. Finally after BT dissolutional widening becomes even and maximal along the central channel which carries the flow through the aquifer. This conduit is surrounded by a fringe of widened fractures, where dissolution has stopped (dark blue and black regions). This behaviour is typical for BT and has already been discussed (Siemers and Dreybrodt, 1998; Gabrovsek, 2000; Dreybrodt and Siemers, 2000).

Here we need it for comparison with the second limiting case illustrated by Fig. 2e–h. Now the lower input has $p_{CO_2}^i = 0.01$ atm and the upper one has $p_{CO_2}^i = 0.05$ atm. The input concentrations of Ca in both inputs are $0.99999c_{eq}$, where c_{eq} is the corresponding equilibrium concentration of Ca with respect to calcite. The evolution of the aquifer is depicted by Fig. 2e–h. In the beginning the head distribution is similar as in Fig. 2a. Fig. 2e shows the aquifer after 10,000 years. Flow still radiates out

from the input points. The two different solutions mix in the central part activating MC. Therefore a conduit starts to grow down-head, where dissolution rates are maximal as indicated by red. As the water flows down head it looses dissolutional power. After 40,000 years (Fig. 2f) the central channel created by MC has reached the output, which is widened continuously until the isoline with $h = 0.1$ m (practically base level) extends entirely along this channel, as is also shown by Fig. 2g (100,000 years) and Fig. 2h (1,500,000 years). Dissolutional widening is finally restricted to this conduit, which grows linear in time.

To further illustrate the evolution of some selected fractures indicated by the arrows 1–6 in Fig. 2g, Fig. 3 shows their aperture widths as they grow in time. In Fig. 3a the evolution of four fractures in the later central channel can be seen. These are indicated by arrows 1–4 in Fig. 2g. Fracture 1 located closest to the input starts to grow first. Fractures 2–4 located further downstream start to grow later in sequence of their locations. Growth rates are high initially and become constant after about 1 million years, when aperture widths of about 50 cm have been reached. These rates amount to 30 cm per million years. Fig. 3b shows the growth of fractures which are abandoned by aggressive solution because they do not belong to the central channel. Their locations are depicted by the arrows 5 and 6 in Fig. 2g. These fractures first grow quickly. After 40,000 and 80,000 years, respectively, they are no longer in the region of MC and growth stops, when aperture widths on the order of 1 cm have been reached. This behaviour is common to all fractures (black colour in Fig. 2e–h) where dissolution has stopped.

The evolution of flow rates through the aquifer for both limiting cases of BT and MC is shown by Fig. 4, curves a and h, respectively. Curve a shows a typical BT behaviour with steeply rising flow rates, because input and output become connected by wide conduits. The behaviour is entirely different for the limiting case with MC active solely (curve h). Dissolutional widening occurs only distant from the inputs where solutions mix. No dissolution is active elsewhere. Higher permeability is created only in this region of MC
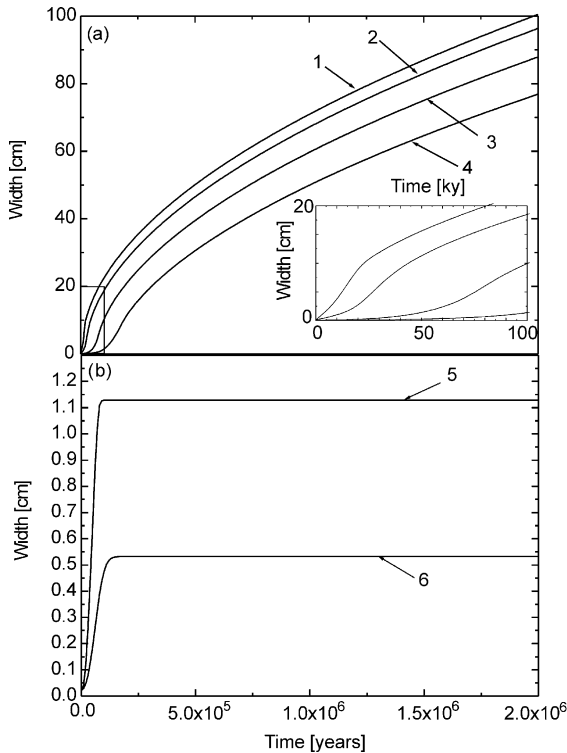
Fig. 3. (a) Evolution of the aperture widths of four selected fractures as depicted by arrows 1–4 in Fig. 2g. All these fractures are located in the central channel, where MC remains active. (b) Evolution of the aperture widths of two fractures, which are abandoned by the action of MC. They are located at the fringe of the central channel as indicated by arrows 5 and 6 in Fig. 2g.

which drains water from the inputs through the system of narrow unwidened fractures. As this region extends down head the flow rates increase. After some time the central area has been integrated to a conduit system with low resistance to flow, extending to the output. Then the not widened fracture system leading water from the inputs to the center determines the flow rates, which become constant after 40,000 years. It should be pointed out here again that the hydrological settings for both runs are identical. Only the difference in the hydrochemical conditions at input B is responsible for the extreme difference of aquifer evolution. Our considerations so far show that two entirely different modes of karstification can be active. The BT mechanism is fast and connects input and output. The MC mode is extremely slow and creates central channels in
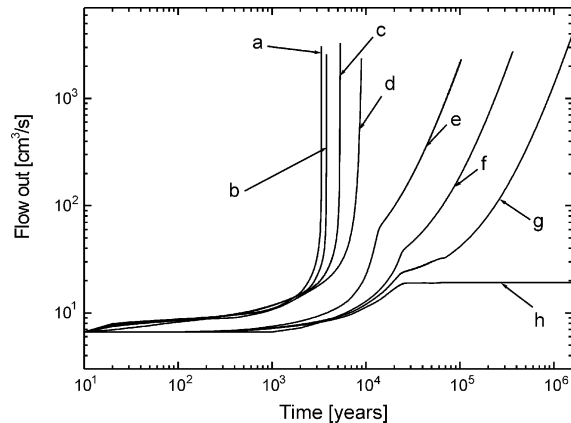

Fig. 4. Flow rates during the evolution of aquifers with identical geological conditions as depicted by the model domain in Fig. 1, but different chemical boundary conditions for the solutions in the upper and lower inputs. (a) $p_{CO_2} = 0.05$ atm and $c_{in} = 0.75c_{eq}$ at both inputs. No MC active. All other curves b–h show the time dependence of flow rates, when $p_{CO_2} = 0.05$ atm at the upper input and $p_{CO_2} = 0.01$ atm at the lower one. Input concentrations are given by $f \times c_{eq}$ with respect to the corresponding equilibrium concentrations at the inputs. (b) $c_{in} = 0.75c_{eq}$, (c) $c_{in} = 0.9c_{eq}$, (d) $c_{in} = 0.96c_{eq}$, (e) $c_{in} = 0.99c_{eq}$, (f) $c_{in} = 0.9925c_{eq}$, (g) $c_{in} = 0.995c_{eq}$, and (h) $c_{in} = 0.99999c_{eq}$ (pure MC).

the order of tenths of centimetres in times of several million years.

5. Intermediate cases between breakthrough and MC

We now combine these two modes in the following scenario. The upper input receives water with $p_{CO_2}^i = 0.05$ atm and $c = 0.75c_{eq}$, $c_{eq} = 2.14 \times 10^{-6}$ mol cm^{-3}, whereas the lower one is fed by a solution with $p_{CO_2}^i = 0.01$ atm, $c = 0.75c_{eq}$, with $c_{eq} = 0.55 \times 10^{-6}$ mol cm^{-3}. Temperature is 10 °C.

The evolution of the aquifer is shown by Fig. 5a–d. After 400 years, similarly as in Fig. 2a and b a conduit starts to grow from the upper input. The water from the lower input, with $p_{CO_2} = 0.01$ atm is considerably less aggressive. Therefore the channel from there has grown only a short distance (Fig. 5a). Fig. 5b represents a new important aspect. In the region close between the two inputs some isolated fractures have grown sufficiently wide by MC. This implies higher hydraulic conductivity in this region.
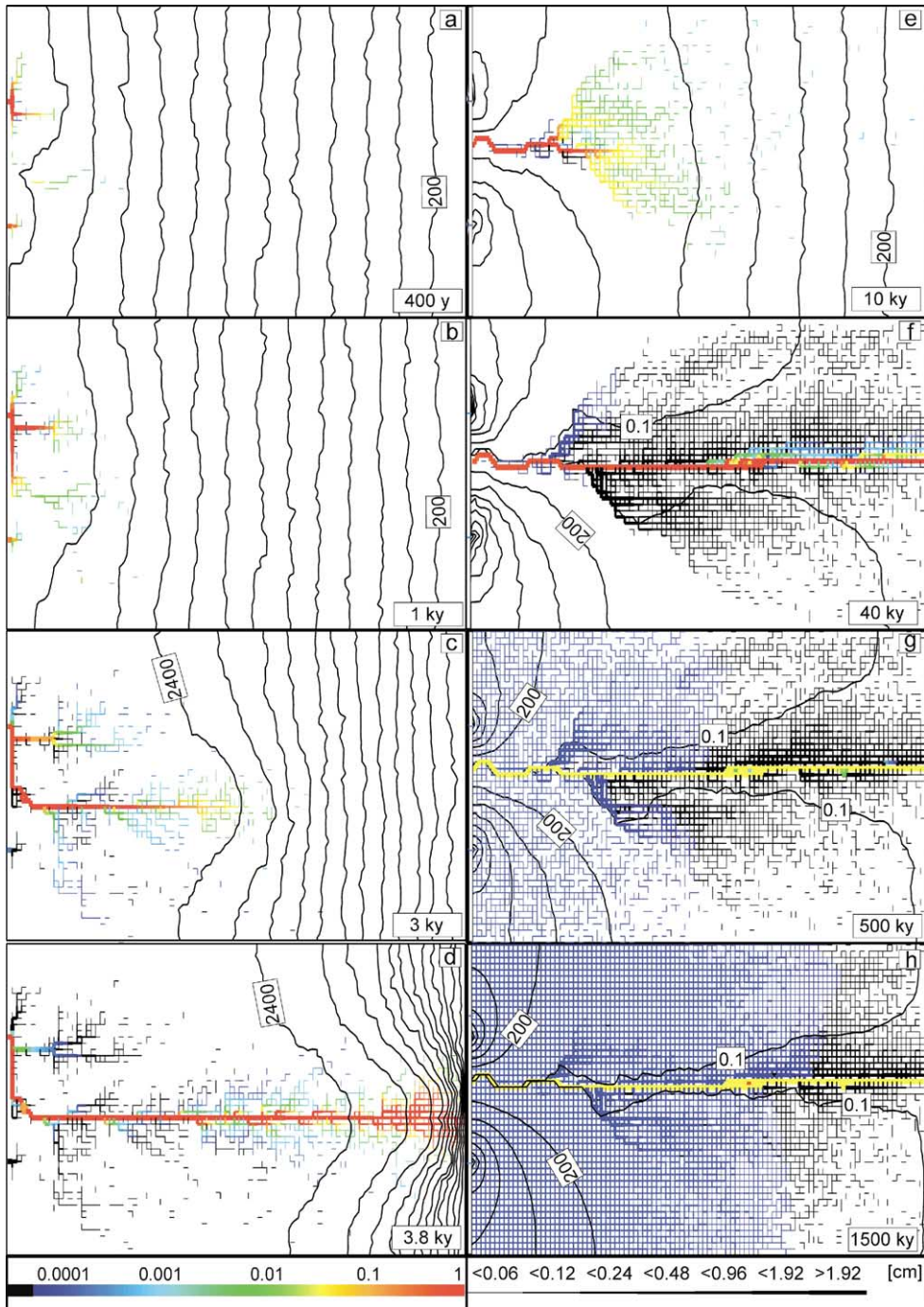
Fig. 5. (a–d) Evolution of dissolution rates and fracture aperture widths for an aquifer dominated by BT-behaviour with MC (see Fig. 4, curve b). (e–h) The evolution of an aquifer dominated by MC and with input solutions exhibiting very low dissolution rates (see Fig. 4, curve g). Bar codes and isolines as in Fig. 2. $F_{max} = 0.00335$ cm/year for (a–d), and $F_{max} = 1.6 \times 10^{-4}$ cm/year for (e–h), respectively.

Therefore the conduit growing from the upper input separates into two branches, with one directed into this area of lower permeability which allows earlier BT. The other keeps its former direction but does not achieve BT. Since MC is active along the center of the aquifer, where waters from the two inputs mix, the lower conduit is more competitive than the upper one. In average aperture widths become larger in the mixing zone than in the region of the upper channel where no MC is active. Therefore the central conduit needs less time for BT (cf. Eqs. (2)–(4)). This is seen in Fig. 5c (3000 years). The lower channel has gained significant lead and BT occurs at 3800 years as illustrated by Fig. 5d. The evolution of flowrates is shown by Fig. 4, curve b. Clearly a BT behaviour is seen, but with the help of MC the pathways of conduit growth are directed into the region where MC is active and therefore are different from those in Fig. 2d, where MC is excluded, but all other conditions are entirely identical. Such a behaviour has already been found by Gabrovsek and Dreybrodt (2000) and by Gabrovsek (2000). Mostly the dissolution rates drop from the input to the output showing that BT behaviour is dominant. Only during the first thousand years MC is active. This can be seen from Fig. 6a which depicts the flow rates into the upper and lower input. The flow into the upper input increases steadily until BT. Due to the redistribution of hydraulic heads, however, flow into the lower input decreases steadily and finally becomes zero. Only in the first thousand years upper and lower flow rates are of similar magnitude, and MC is active. After that time MC is switched off, because flow into the lower input becomes negligible and the entire aquifer is fed by the upper input.

One expects that the influence of the BT mechanism is reduced, when the input solutions become closer to saturation. To this end we have performed computer runs with c_{in} increasing from $0.75c_{eq}$, $0.9c_{eq}$, $0.96c_{eq}$, $0.99c_{eq}$, $0.9925c_{eq}$, and $0.995c_{eq}$ (curves b–g) in Fig. 4, respectively. Curves a–d exhibit typical BT behaviour and the evolution of the respective aquifer is similar to that shown by Figs. 2a–d and 5a–d. As the input solution comes closer to equilibrium, $c_{in} \geq 0.99 \times c_{eq}$ the pattern of flow evolution changes as shown by curves e–g. All curves first exhibit a steady increase of flow rates, but do not show BT as curves a–d. For $c_{in} = c_{eq}$, when
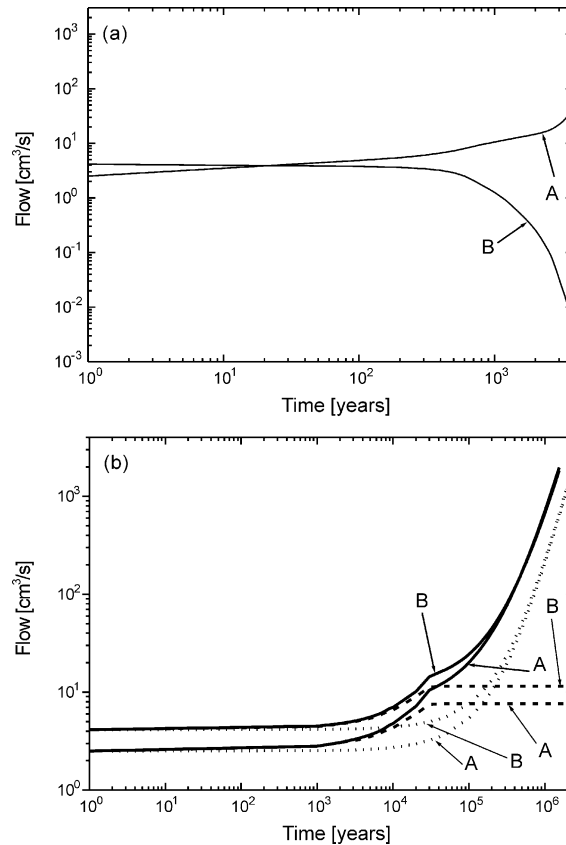

Fig. 6. (a) Evolution of flow rates at the inputs A and B for BT-behaviour. (b) Evolution of flow rates at inputs A and B for MC dominated aquifers. Full lines: flow rates for the aquifer shown by Fig. 5e–h, see also Fig. 4, curve g. Dashed lines: pure MC-behaviour, see Fig. 2e–h and also Fig. 4h. Dotted lines: MC is switched off by using equal chemical compositions at both inputs. ($p_{CO_2} = 0.05$ atm, $c_{in} = 0.995c_{eq}$). The initial steep rise for MC-dominated aquifers (full lines) is missing because MC is not active.

only MC is active (curve h) flow rates become constant. Evidently BT does no longer dominate the evolution of the aquifer.

This is illustrated by Fig. 5e–h, which show the evolution for $c_{in} = 0.995c_{eq}$. During the first 40,000 years the evolution of the aquifer is almost identical to that of pure MC, as shown by Fig. 2e–f. This can be seen by comparison of Fig. 2e with Fig. 5e, both at 10,000 years. Dissolution rates are so low at the entrances that this time is not sufficient to allow dissolutional widening to a noticeable extent. The evolution of the aquifer departs at times of several 100,000 years. This is seen from the system of

fractures (blue) which extend from the input after 500.000 years (Fig. 5g) and 1.5 million years (Fig. 5h). On such time scales dissolutional widening from the slightly undersaturated input solution opens those fractures, where MC remains absent, by several times of their initial values of aperture width. Therefore, in contrast to pure MC, where this is not the case, flow rates increase continuously.

More insight into the evolution is obtained by inspection of the flow rates into the upper (A) and the lower (B) inputs, illustrated by Fig. 6b, full lines. In contrast to the BT behaviour shown in Fig. 6a both flow rates increase with values of similar magnitude, such that MC is maintained over all times.

In the first stage of the evolution, when the region of increasing permeability progresses towards the output a steep increase in flow rates is observed. After the channel has reached the output the flow rates are determined by the flow through the narrow fractures of the net. Dissolutional widening is still active everywhere and even in the net of narrow fractures because of the high input concentration (cf. Eqs. (2) and (3)). This is the reason for the further increase in flow rates. See also Fig. 4 (curve g). If this dissolutional widening is switched off by employing an input concentration of $0.99999c_{eq}$ as in the limiting case of MC only (see Fig. 2e–h), the flow rates become constant in time. This is also illustrated in Fig. 6b, where the flow rates for this case are shown in addition (dashed lines). At the beginning they are identical to those when slow dissolutional widening is active because MC is dominating during the first 40,000 years.

Another confirmation of dissolutional widening in the net can be found by switching off MC, choosing equal $p_{CO_2}^i$ for both inputs. The evolution of flow rates is depicted in Fig. 6b (dotted lines). The early steep increase is missing since no channel develops when MC is switched off. But since dissolutional widening is low and even in the entire net flow rates begin to increase after 40,000 years.

In summary: Two basic patters of flow evolution have been found. As can be seen from Fig. 4, curves a–d are entirely controlled by a feedback mechanism leading to BT. Increasing flow rates induce increasing dissolution rates and vice versa until the sudden increase in flow rates happens. The evolution of flow rates for curves e–g is entirely different. Flow rates

increase as the channel propagates downhead. But there is no increase in dissolution rates as flow increases, because dissolution rates are now determined by MC. After the channel has reached the downhead boundary of the aquifer, flow rates are determined entirely by the hydraulic resistance of the fractures, connecting the input points to the central channel. As stated above dissolution rates there are constant in time and space. Therefore all those fractures widen linearly in time with equal rates. Consequently flow rates increase by time cubed (t^3). Therefore a feedback mechanism is absent for curves e–f, and of course also for curve h, where the input solutions are at saturation and dissolutional widening of the connecting fractures is not possible.

6. Discussion

The modelling results have revealed two modes of karstification which act simultaneously; MC and BT-behaviour. BT is dominating when the solutions are highly aggressive and mixing of two solutions with different chemistry does not change the dissolution rate in a significant way. On the other hand if the waters entering the karst system are close to saturation $c_{in} \geq 0.99c_{eq}$ their dissolution rates are very low. An increase in hydraulic conductivities in the net by one order of magnitude (i.e. widening of the fractures to twice their initial aperture widths) takes about 20,000 years for $c_{in} \geq 0.99c_{eq}$, but already 300,000 years for $c_i = 0.995c_{eq}$. Dissolution rates arising by MC are higher by orders of magnitude ($F_{max} \approx 10^{-13} \, \mathrm{mol \, cm^{-2} \, s^{-1}}$), and they govern the evolution of the aquifer. By this way, solely from the chemistry of the inflowing solutions, an aquifer evolves quite differently, although all other details are kept fixed. In all our computer runs only the concentrations of CO_2 at input B and the input saturation ratios were changed.

To illustrate the various differences in the properties of the aquifers, Fig. 7 shows cartoons of their fracture widths from the pure BT-type to the pure MC-type aquifers in the order of increasing input concentrations. The corresponding evolution of flow rates is shown by Fig. 4, curves a–h, respectively. Fig. 7a shows the typical BT aquifer with no MC active since at both inputs $p_{CO_2} = 0.05$ atm. Its main
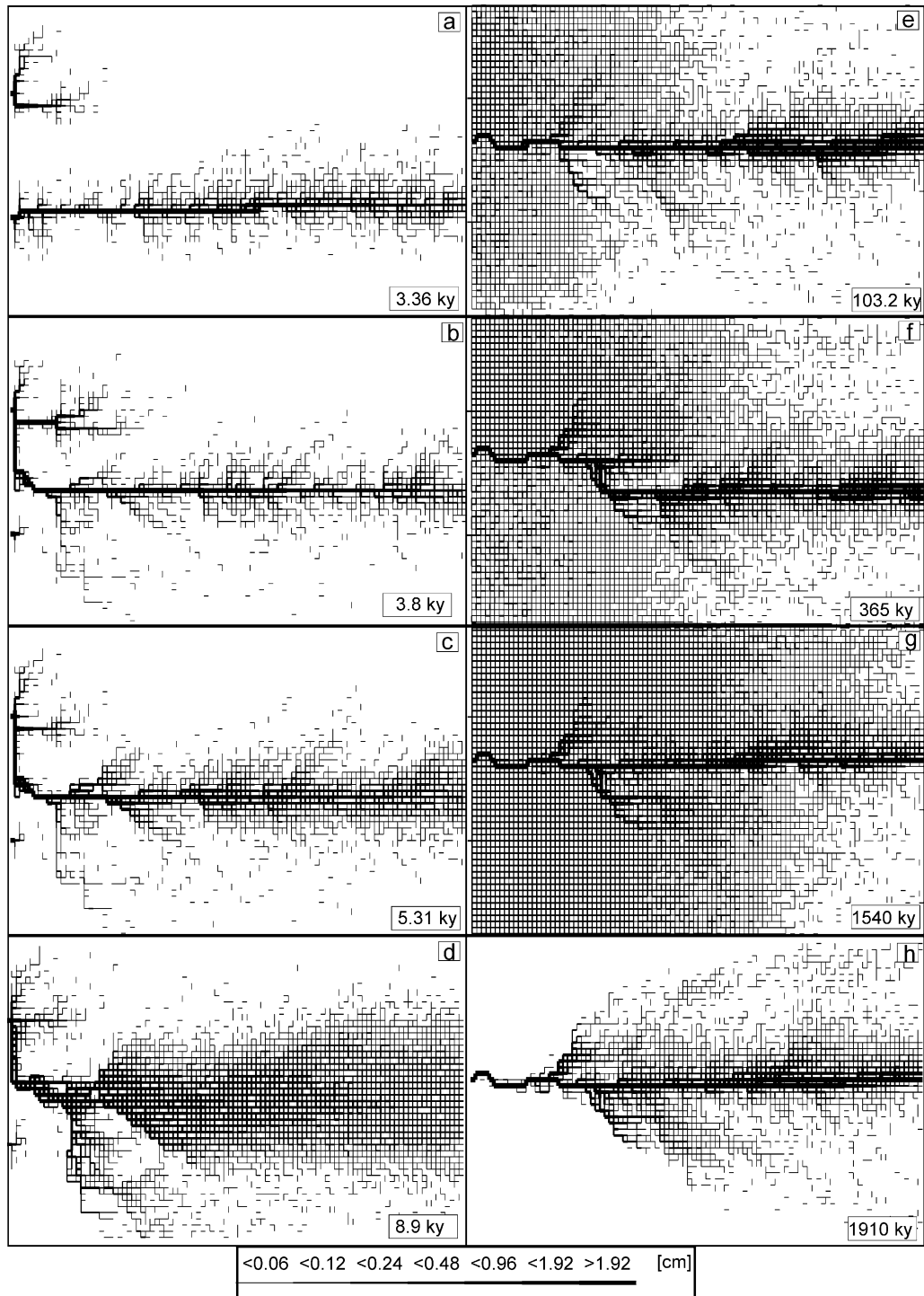
Fig. 7. Aperture widths of all aquifers, at the terminations of the model runs. The letters in the figures relate to the corresponding curves in Fig. 4. Aquifers a-d are BT-dominated, whereas aquifers e–g are controlled by MC.

conductivity is presented by the channels which are surrounded by a fringe of fractures, where solution, still aggressive, flows from the central fracture into the net. Most of the aquifer, more distant from this conduit however, does not exhibit any significant change in fracture widths and flow is almost entirely concentrated through the karst conduits. Fig. 7b shows the action of MC by changing the p_{CO_2} at the lower input to 0.01 atm leaving everything else unchanged. As has been described by Fig. 5a–d MC creates increased permeability which diverts the conduit growing from the upper channel into this region. We also observe a fringe of widened channels along these conduits, but more distant regions remain unaltered. In Fig. 7c the input concentration is increased to $0.90c_{eq}$, and MC gains in influence. The solutions flowing out from the conduits mix with those in the fractures. Thus the fringe of widened fractures surrounding the conduits extends, and shapes a complicated dentritic pattern. This behaviour is intensified if the influence of MC is increased by further increase of c_{in} to $0.96c_{eq}$ (Fig. 7d). An entirely different aquifer is created for $c_i = 0.99c_{eq}$ (Fig. 7e) (note, the input dissolution rates drop as $(1 - c_{in}/c_{eq})^4$). MC creates a channel in the central part where the two input solutions mix. Due to the low dissolution rates of the inflowing solutions there is no direct connection to the upper input. Because of the high resistance of the narrow fractures connecting the input to the central channel constant head conditions can be maintained for long times ($t = 103,200$ years). This time is sufficient to widen those input fractures by the small, but within this time scale, sufficient dissolutional power of the input solutions. In contrast to Fig. 7a–d the left hand side region close to the input exhibits significant hydraulic conductivities. The channel no longer shows the fringe of widened fractures, rather than a much wider region of wide conduits created by MC. In the BT cases aggressive water is injected from the channels to the net during the early stage of the evolution. This is not possible for MC-type evolution because the hydraulic head along the channel is very low. Therefore water entering the channels from the net widens the channels by MC. A similar behaviour is depicted in Fig. 7f and g, where c_{in} has been increased to 0.9925 and to 0.995, respectively. Due to the high input concentrations the time to create permeability in

the areas surrounding the inputs becomes longer, but the general pattern does not change. By injecting input solutions at equilibrium, dissolution can occur only by MC, as illustrated in Fig. 7h. Since mixing is excluded in the region close to the inputs hydraulic conductivity remains unchanged, and flow into the channel created by MC becomes constant.

In summary comparison of the structure of the aquifers in Fig. 7 reveals that a complex interplay between BT-processes and MC creates aquifers with largely different properties.

One final comment should be given here. Our modelling scenario is highly idealistic. In contrast to nature it assumes that the chemical composition of the input solution is constant during the time of the model runs. It further assumes that the location of the input points do not change with time. Limitation of computation requires a highly idealistic fracture network. Under such highly idealized conditions such models cannot reflect all details which are observed in natural caves. As an example Fig. 7 exhibits straight channels, which do not exhibit sinuosity as often observed in nature. However, the purpose of our modelling efforts is not to simulate natural caves but to find the mechanisms which can be active during their evolution. MC is just one of them. It does not wonder therefore that a model which is built to extract the influence of only one mechanism cannot reflect the full variety observed in nature, where many mechanisms are active simultaneously.

7. Conclusion

The evolution of karst aquifers depends in a complex way on the manifold boundary conditions, such as geological settings, hydrologic properties of the initial aquifers and petrologic properties of the limestone as shown by many modelling efforts. Here we consider an up to now not intensively investigated field which deals with the impact of the chemistry of water flowing into an evolving karst aquifer. A simple domain with two symmetrical inputs of chemically different waters under constant head conditions is examined. If these waters are allogenic, well distant from equilibrium with respect to calcite, two competitive channels grow downstream. As soon as

the more competitive one wins the race in reaching the output boundary at low head a dramatic increase in flow at this BT event is observed.

On the other hand autogenic water close to saturation may enter from limestone areas into a karstifiable geological setting. In the extreme case, when the solutions are fully saturated, but with different equilibrium concentrations, dissolution of limestone is possible, where these waters mix someplace within the initial aquifer and renewed undersaturation is created by MC. In such a case integrated channels grow at a much slower pace, which receive water from the fracture system close to the inputs, where no dissolution and consequently no widening occurs. These channels propagate downstream and finally reach base level. After several million years they have grown to conduits with a diameter of 50 cm. Evidently the combination of MC and the nonlinear dissolution kinetics of limestone can create conduits in karst aquifers, although at a much slower pace in comparison to the BT mode of karstification.

We have examined the combination of these two modes by systematically changing the input concentrations from 0.75 to $0.9999c_{eq}$. For sufficiently low input concentrations up to $0.99c_{eq}$ the BT behaviour dominates although significantly modified by the increasing influence of MC. For higher input concentrations MC creates a central channel, but slow dissolutional widening of the entrance fracture increases flow rates and the efficiency of MC. Although in all runs everything was kept identical and only the chemistries of the input waters were changed aquifers with significantly different hydrologic properties result.

References

Bögli, A., 1980. Karst Hydrology and Physical Speleology, Springer, Berlin.

Clemens, T., Hückinghaus, D., Sauter, M., Liedl, R., Teutsch, G., 1997. Modelling the genesis of karst aquifer systems using a coupled reactive network model, Hard Rock Geosciences, IAHS Publications 241, Colorado, pp. 3–10.

Clemens, T., Hückinghaus, D., Liedl, R., Sauter, M., 1999. Simulation of the development of karst aquifers: the role of epikarst. International Journal of Earth Sciences 88, 157–162.

Dreybrodt, W., 1988. Processes in Karst Systems—Physics Chemistry and Geology, Springer Series in Physical Environments, vol. 4. Springer, Berlin.

Dreybrodt, W., 1990. The role of dissolution kinetics in the development of karstification in limestone. A model simulation of karst evolution. Journal of Geology 98, 639–655.

Dreybrodt, W., 1996. Principles of early development of karst conduits under natural and man-made conditions revealed by mathematical analysis of numerical models. Water Resources Research 32, 2923–2935.

Dreybrodt, W., Eisenlohr, L., 2000. Limestone dissolution rates in karst environments. In: Klimchouk, A., Ford, D.C., Palmer, A.N., Dreybrodt, W. (Eds.), Speleogenesis: Evolution of Karst Aquifers, National Speleological Society, USA.

Dreybrodt, W., Gabrovsek, F., 2000. Dynamics of the evolution of a single karst conduit. In: Klimchouk, A., Ford, D.C., Palmer, A.N., Dreybrodt, W. (Eds.), Speleogenesis: Evolution of Karst Aquifers, National Speleological Society, USA.

Dreybrodt, W., Siemers, J., 2000. Cave evolution on two-dimensional networks of primary fractures in limestone. In: Klimchouk, A., Ford, D.C., Palmer, A.N., Dreybrodt, W. (Eds.), Speleogenesis: Evolution of Karst Aquifers, National Speleological Society, USA.

Eisenlohr, L., Meteva, K., Gabrovšek, F., Dreybrodt, W., 1999. The inhibiting action of intrinsic impurities in natural calcium carbonate minerals to their dissolution kinetics in aqueous H_2O-CO_2 solutions. Geochimica et Cosmochimica Acta 63, 989–1002.

Ford, D.C., Williams, P.W., 1989. Karst Geomorphology and Hydrology, Unwin Hyman, London.

Gabrovsek, F., 2000. Evolution of early karst aquifers: from simple principles to complex models. Institut za raziskovanje krasa ZRC SAZU, Zalozba ZRC, Ljubljana

Gabrovsek, F., Dreybrodt, W., 2000. The role of mixing corrosion in calcite aggressive $H_2O-CO_2-CaCO_3$ solutions in the early evolution of karst aquifers. Water Resources Research 36, 1179–1188.

Gabrovsek, F., Dreybrodt, W., 2001. A model of the early evolution of karst aquifers in limestone in the dimensions of length and depth. Journal of Hydrology 240, 206–224.

Groves, C.G., Howard, A.D., 1994. Early development of karst systems 1. Preferential flow path enlargement under laminar flow. Water Resources Research 30, 2837–2846.

Howard, A.D., Groves, C.G., 1995. Early development of karst systems. 2. Turbulent flow. Water Resources Research 31 (1), 19–26.

Kaufmann, G., Braun, J., 1999. Karst aquifer evolution in fractured rocks. Water Resources Research 35, 3223–3238.

Kaufmann, G., Braun, J., 2000. Karst aquifer evolution in fractured, porous rocks. Water Resources Research 36, 1381–1391.

Laptev, F.F., 1939. Aggressive action of water on carbonate rocks, gypsum, and concrete. GONTI, Moscow-Leningrad, 120 p (in Russian)

Palmer, A.N., 1984. Recent trends in karst geomorphology. Journal of Geological Education 32, 246–253.

Palmer, A.N., 1991. The origin and morphology of limestone caves. Geological Society of America Bulletin 103, 1–21.

Palmer, A.N., 1999. Patterns of dissolution porosity in carbonate rocks. Karst Waters Institute, Special Publication 5.

Palmer, A.N., 2000. Digital modeling of individual solution conduits. In: Klimchouk, A., Ford, D.C., Palmer, A.N., Dreybrodt, W. (Eds.), Speleogenesis: Evolution of Karst Aquifers, National Speleological Society, USA.

Siemers, J., Dreybrodt, W., 1998. Early development of karst aquifers on percolation networks of fractures in limestone. Water Resources Research 34, 409–419.

Svensson, U., Dreybrodt, W., 1992. Dissolution kinetics of natural calcite minerals in CO_2–water systems approaching calcite equilibrium. Chemical Geology 100, 129–145.

White, W.B., 1988. Geomorphology and Hydrology of Karst Terrains, Oxford University Press, New York.

Worthington, S.R.H., Ford, D.C., Beddows, O.A., 2000. Porosity and permeability enhancement in unconfirmed carbonate aquifers as a result of solution. In: Klimchouk, A., Ford, D.C., Palmer, A.N., Dreybrodt, W. (Eds.), Speleogenesis: Evolution of Karst Aquifers, National Speleological Society, USA.